ORGANIC MOLECULES IN THE GALACTIC CENTER.[*]

HOT CORE CHEMISTRY WITHOUT HOT CORES.

M. A. Requena-Torres[1], J. Martín-Pintado[1], A. Rodríguez-Franco,[1][2] S. Martín[3], N. J. Rodríguez-Fernández[4], and P. de Vicente[5]

[1] Departamento de Astrofísica Molecular e Infrarroja, Instituto de Estructura de la Materia-CSIC C Serrano 121, E-28006 Madrid, Spain
e-mail: requena@damir.iem.csic.es
[2] Escuela Universitaria de Óptica, Departamento de Matemática Aplicada (Biomatemática), Universidad Complutense de Madrid, Avenida Arcos de Jalón s/n, E-28037 Madrid, Spain.
[3] Instituto de Radioastronomía Milimétrica Av. Divina Pastora 7, Local 20, E-18012 Granada, Spain e-mail: martin@iram.es
[4] Observatoire de Bordeaux, L3AB (UMR 5804), CNRS/Université Bordeaux 1, BP 89, 2 rue de l'Observatoire, 33270 Floirac, France
e-mail: nemesio.rodriguez@obs.u-bordeaux1.fr
[5] Observatorio Astronómico Nacional, Centro Astronómico de Yebes Apartado 148, 19080 Guadalajara, Spain e-mail: p.devicente@oan.es

ABSTRACT

Aims. We study the origin of large abundances of complex organic molecules in the Galactic center (GC).
Methods. We carried out a systematic study of the complex organic molecules CH_3OH, C_2H_5OH, $(CH_3)_2O$, $HCOOCH_3$, $HCOOH$, CH_3COOH, H_2CO, and CS toward 40 GC molecular clouds. Using the LTE approximation, we derived the physical properties of GC molecular clouds and the abundances of the complex molecules.
Results. The CH_3OH abundance between clouds varies by nearly two orders of magnitude from 2.4×10^{-8} to 1.1×10^{-6}. The abundance of the other complex organic molecules relative to that of CH_3OH is basically independent of the CH_3OH abundance, with variations of only a factor 4–8. The abundances of complex organic molecules in the GC are compared with those measured in hot cores and hot corinos, in which these complex molecules are also abundant. We find that both the abundance and the abundance ratios of the complex molecules relative to CH_3OH in hot cores are similar to those found in the GC clouds. However, hot corinos show different abundance ratios than observed in hot cores and in GC clouds. The rather constant abundance of all the complex molecules relative to CH_3OH suggests that all complex molecules are ejected from grain mantles by shocks. Frequent ($\sim10^5$ years) shocks with velocities $>6\,km\,s^{-1}$ are required to explain the high abundances in gas phase of complex organic molecules in the GC molecular clouds. The rather uniform abundance ratios in the GC clouds and in Galactic hot cores indicate a similar average composition of grain mantles in both kinds of regions. The Sickle and the Thermal Radio Arches, affected by UV radiation, show different relative abundances in the complex organic molecules due to the differentially photodissociation of these molecules.

Key words. Astrochemistry – ISM: clouds – ISM: molecules – Radio lines: ISM – Galactic: center

1. Introduction

Gas-grain interaction in the interstellar medium (ISM) can have a large impact on its chemistry because of the desorption and/or depletion of molecules onto grains mantles. The gas phase abundance of molecules, which are believed to be efficiently formed on dust grains such as, methanol (CH_3OH), ethanol (C_2H_5OH), and formaldehyde (H_2CO), can be enhanced by orders of magnitude due to the ejection/evaporation of these molecules from grain mantles.

One of the interesting features of the gas-phase chemistry after ejection of these molecules is the fast conversion of these parent molecules into daughter molecules. The relative abundance of dimethyl ether ($(CH_3)_2O$) is expected to change by three orders of magnitude in a short period of time after CH_3OH is ejected to gas phase (Millar et al. 1991; Caselli et al. 1993; Charnley et al. 1995; Horn et al. 2004). Basically all models of alcohol-driven chemistry have indicated that $(CH_3)_2O$ and methyl formate ($HCOOCH_3$) will reach their largest abundances 10^4-10^5 years after the ejection of CH_3OH into gas phase. However, Horn et al. (2004) have shown that $HCOOCH_3$ formation in gas phase from CH_3OH is less efficient than previously considered in the models. This casts some

[*] Table 7 is only available in electronic at the CDS via anonymous ftp to cdsarc.u-strasbg.fr (130.79.125.5) or via http://cdsweb.u-strasbg.fr/Abstract.html

doubts on the gas-phase production of $HCOOCH_3$, and they propose that this molecule is also formed on grain mantles. The gas phase/grain formation of $(CH_3)_2O$ has been studied by Peeters et al. (2006), showing that the main path to form $(CH_3)_2O$ is by gas-phase reactions and that its formation on grains is a minor source of the observed abundances. Other organic molecules like formic acid (HCOOH) can be produced in both gas phase and grain mantle chemistry (Liu et al. 2002).

So far, large abundances of complex molecules have been detected in three different kinds of objects: hot cores associated with massive star formation (Ikeda et al. 2001), hot corinos associated with low-mass star formation (Bottinelli et al. 2006), and the Galactic center (GC) clouds (Martín-Pintado et al. 2001). Their physical properties are very different. While the hot cores and hot corinos are small ($\lesssim 0.1$ pc), hot (>100 K), and very dense ($\gtrsim 10^5$ cm^{-3}) condensations, the GC molecular clouds show averaged scales of 20-30 pc, kinetic temperatures $\sim$50-200 K, and an averaged density of $\sim 10^4$ cm^{-3} (Güsten & Philipp 2004). The molecular gas in the inner region of our Galaxy presents a different chemistry than in the Galactic disk (Martín-Pintado et al. 1997). In the GC, widespread large abundances of grain-processed molecules like CH_3OH, C_2H_5OH, and silicon monoxide (SiO) are observed (Gottlieb et al. 1979; Minh et al. 1992; Martín-Pintado et al. 1997, 2001; Hüttemeister et al. 1998). It has been proposed that the sputtering of grains and grain mantles produced by widespread shocks with moderated velocities of ≤ 40 km s^{-1} are the responsible of the "rich" chemistry observed in the GC clouds. The origin of the large scale shocks is so far unclear. These shocks could be produced by cloud-cloud collisions associated with the large-scale dynamics in the context of a barred potential (Hasegawa et al. 1994; Hüttemeister et al. 1998; Rodríguez-Fernández et al. 2006), by wind-blown bubbles driven by evolved massive stars (Martín-Pintado et al. 1999), or by hydrodynamic (HD) or magneto hydrodynamic turbulence (MHD) (Morris & Serabyn 1996). Since the formation of some complex organic molecules is believed to proceed in gas phase after the passage of the shocks and their abundances rapidly evolve, one could use the abundances of these molecules to gain insight into the chemistry of complex molecules in the ISM and to constrain the age of shocks in the GC (Martín-Pintado et al. 2001).

Following these ideas we made a systematic study of 40 molecular clouds in the GC region, between Sgr B2 and Sgr C, in complex molecules believed to be formed on grains like CH_3OH, C_2H_5OH, and $HCOOCH_3$, in gas phase from CH_3OH like $(CH_3)_2O$ and in gas phase and/or grains like HCOOH and H_2CO. We also searched for the less abundant isomer of $HCOOCH_3$, the acetic acid (CH_3COOH). As tracers of the total column density of the molecular gas, we observed molecules like $C^{18}O$, ^{13}CO, and CS. Our systematic study shows that all the complex organic molecules present similar relative abundances with respect to CH_3OH, except for the regions where photodissociation could be important. Furthermore, the abundance and abundance ratios of these complex molecules in the GC are similar to those observed in hot cores, while hot corino abundances seem to have similar ratios for different objects. Our results suggest that all complex organic molecules have

Table 1. Molecular line parameters

Molecule	Transition	Frequency (MHz)	E_u/κ (K)	$\mu_x^2 S$
CH_3OH.......	$3_0 \rightarrow 2_0$ E	145093.75	27.06	2.38
	$3_{-1} \rightarrow 2_{-1}$ E	145097.47	19.52	2.11
	$3_0 \rightarrow 2_0$ A+	145103.23	13.94	2.38
	$5_0 \rightarrow 4_0$ E	241700.22	47.95	3.91
	$5_{-1} \rightarrow 4_{-1}$ E	241767.22	40.41	3.75
	$5_0 \rightarrow 4_0$ A+	241791.43	34.83	4.94
$^{13}CH_3OH$ ...	$3_{03} \rightarrow 2_{02}$ E	141595.48	26.71	2.43
	$3_{-13} \rightarrow 2_{-12}$ E	141597.06	19.21	2.16
	$3_{03} \rightarrow 2_{02}$ A+	141602.53	13.60	2.43
C_2H_5OH	$4_{14} \rightarrow 3_{03}$	90117.61	9.36	5.35
	$7_{07} \rightarrow 6_{16}$	104487.26	23.26	8.61
	$9_{09} \rightarrow 8_{18}$	142285.05	37.17	12.66
$HCOOCH_3$ ..	$7_{25} \rightarrow 6_{24}$ E	90145.69	19.69	17.00
	$7_{25} \rightarrow 6_{24}$ A	90156.48	19.67	17.00
	$8_{08} \rightarrow 7_{07}$ E	90227.61	20.09	20.99
	$8_{08} \rightarrow 7_{07}$ A	90229.63	20.07	20.99
	$9_{45} \rightarrow 8_{44}$ E	111408.48	37.27	19.13
	$9_{18} \rightarrow 8_{17}$ E	111674.10	28.15	23.12
	$9_{18} \rightarrow 8_{17}$ A	111682.19	28.13	23.12
$(CH3)_2O^a$	$7_{26} \rightarrow 7_{17}$	104703.30	31.07	5.43
	$7_{07} \rightarrow 6_{16}$	111783.01	25.26	6.80
HCOOH	$4_{22} \rightarrow 3_{21}$	90164.25	23.53	5.78
	$5_{05} \rightarrow 4_{04}$	111746.79	16.13	9.65
CH_3COOH ..	$8_{*8} \rightarrow 7_{*7}$ A	90246.25	20.30	43.20
	$8_{*8} \rightarrow 7_{*7}$ E	90203.44	20.30	43.20
	$10_{*10} \rightarrow 9_{*9}$ A	111548.53	30.50	54.80
	$10_{*10} \rightarrow 9_{*9}$ E	111507.27	30.50	54.80
CS	$3 \rightarrow 2$	146969.03	14.12	11.56
	$5 \rightarrow 4$	244936.64	35.28	19.84
$C^{18}O$	$1 \rightarrow 0$	109782.17	5.28	0.01
	$2 \rightarrow 1$	219560.35	15.82	0.02
^{13}CO	$1 \rightarrow 0$	110201.35	5.30	0.01
$H_2^{13}CO$	$2_{02} \rightarrow 1_{01}$	141983.74	7.11	10.87

^{a} EE, AA, EA, and AE substates blended. Only the most intense transition is given.

been ejected from grain mantles and that their abundances represent, in first approximation, the grain mantle composition.

2. Observations and results

The observations of all transitions of the complex organic molecules shown in Table 1 were carried out with the IRAM 30-m radio telescope at Pico Veleta (Spain). The data were obtained in different seasons between 1996 and 2003. The half-power beam width of the telescope was 24″, 17″, and 12″ for the 3, 2, and 1.3 mm bands. The receivers, equipped with SIS mixers, were tuned to single sideband with image rejections $\gtrsim 10$ dB. The typical system temperatures were 300, 500, and 900 K for the 3, 2, and 1.3 mm lines, respectively. We used two filterbanks of 256 x 1 MHz and one of 512 x 1 MHz as spectrometers. The velocity resolutions provided by the filter banks were 3, 2, and 1.3 km s^{-1} for the 3, 2, and 1.3 mm bands, respectively. Spectra were calibrated using the standard dual load system. We used the antenna temperature scale (T_A^*) for the line
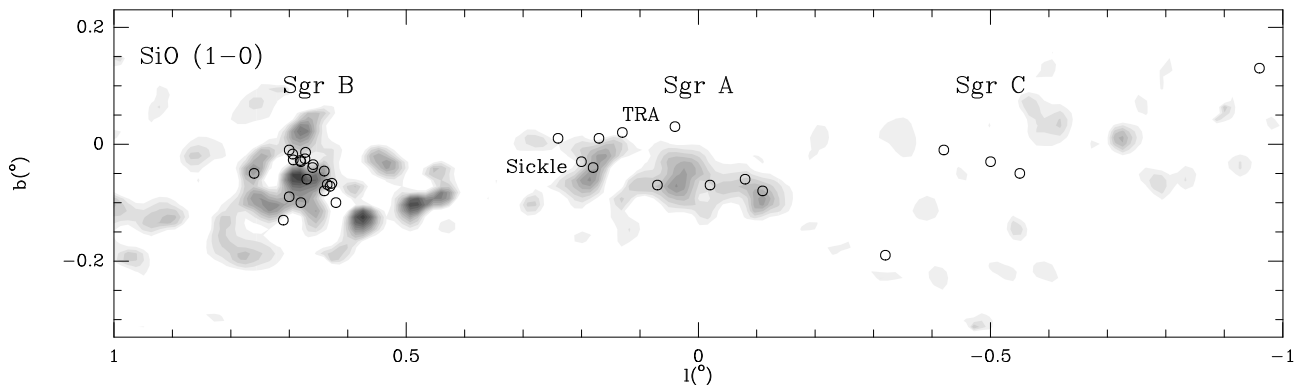
Fig. 1. Position of the observed sources superimposed on the SiO J=1→0 maps from the GC region by (Martín-Pintado et al. 1997).

intensities because the emission is rather extended and completely fills the beam.

Figure 1 shows the location of the sources we observed superimposed on the large-scale SiO map of the GC by Martín-Pintado et al. (1997). The sources were selected from the SiO maps of Martín-Pintado et al. (1997). Some of these sources had already been observed in C_2H_5OH by Martín-Pintado et al. (2001). We also included some clouds in Sgr C, the Thermal Radio Arches (TRA) (Serabyn & Güsten 1987), and the Sickle (Serabyn & Güsten 1991), where the C_2H_5OH emission was not detected by Martín-Pintado et al. (2001). The selected molecular clouds are spread over the region between Sgr C and Sgr B2. The positions of the sources are given in galactic and equatorial coordinates in Table 2. The nomenclature used to designate them is similar to that of Martín-Pintado et al. (2001): MC stands for Molecular Cloud followed by a G and the galactic coordinates, as recommended by the IAU. We grouped the sources in different regions as shown in Fig. 1 and Table 2.

Figures 2 and 3 show samples of line profiles for all observed molecules toward selected sources. Only for some sources like MC G−0.02−0.07 we did observe all the molecular lines. The line profiles of molecules such as CH_3OH are different from those of the CO isotopomers and CS due to the blending of several transitions. The complex organic molecules were only detected in some of the velocity components observed in $C^{18}O$, ^{13}CO, and CS. A good example of this difference in line profiles is shown in Figs. 2 and 3 for the source MC G+0.76−0.05 where $C^{18}O$, ^{13}CO, and CS show three or more velocity components, but C_2H_5OH only shows one. Each velocity component has been treated as an independent molecular cloud. Multiple velocity components are also found toward MC G+0.13+0.02, MC G+0.18−0.04, and MC G−0.32−0.19.

3. Analysis of the data

To derive the physical and chemical properties of the selected molecular clouds, we fitted Gaussian profiles to all detected molecular lines for each velocity component. The observed spectra of some organic molecules are more complex than a single Gaussian profile because of the overlap of several transitions due to the large linewidths observed toward the GC

clouds. To account for the overlap, we used the following constrains for the Gaussian fitting depending on the observed transitions:

– For molecules without internal rotation, like CS, $C^{18}O$, ^{13}CO, HCOOH, and $H_2^{13}CO$, and for molecules with internal rotation when the transitions are sufficiently separated, like those of C_2H_5OH and some of the $HCOOCH_3$ lines, simple Gaussian profiles were fitted to each transition for every velocity component. As mentioned before, the CS, $C^{18}O$, and ^{13}CO profiles generally show more velocity components than those observed in the complex organic molecules. For this work we only fitted the components in the velocity range where at least one organic molecule was detected. In the case where the velocity components overlapped we calculated the integrated intensity of CS, $C^{18}O$, and ^{13}CO in the velocity range where the complex organic molecules show the emission.

– The CH_3OH and $^{13}CH_3OH$ profiles are composed of several overlapped transitions arising from levels at different energies. In this case, we fitted the blended transitions with multi-Gaussian profiles forced to have the same linewidth and velocity separations corresponding to the rest frequencies of the transitions. We also forced the relative intensities derived from the spectroscopic parameters (Tables 1 and 3), assuming the same rotational temperature for all the transitions. In addition to the radial velocity and linewidth, we also fitted the rotational temperature and the optical depths that match the observed profiles. In this case, the antenna temperatures were obtained from $(T_{rot}-T_{bg})(1-e^{-\tau})$. We used the optically thin emission from $^{13}CH_3OH$ transitions to test the optical depths and the antenna temperatures obtained from the CH_3OH fits. The optical depths derived from the CH_3OH lines are in good agreement with those obtained from the [CH_3OH/$^{13}CH_3OH$] line-intensity ratios, assuming a $^{12}C/^{13}C$ ratio of 20 (Wilson & Rood 1994). For the $^{13}CH_3OH$, and in some cases for the CH_3OH lines, only the transitions with the largest intensities were fitted. In the case of the CH_3OH 5_0→4_0E transition, a simple Gaussian fit was made since this line is not overlapped with any other transition.

– Due to its internal rotation, the $(CH_3)_2O$ rotational levels are split into four substates with similar Einstein coefficients

Table 2. Source position

source	l(^{o})	b(^{o})	α (B1950)	δ (B1950)	Region
MC G−0.96+0.13	−0.96	+0.13	$17^h\ 39^m\ 36^s6$	-29° 39′ 47″	Sgr C
MC G−0.55−0.05	−0.55	−0.05	$17^h\ 41^m\ 20^s0$	-29° 24′ 30″	Sgr C
MC G−0.50−0.03	−0.50	−0.03	$17^h\ 41^m\ 21^s2$	-29° 21′ 26″	Sgr C
MC G−0.42−0.01	−0.42	−0.01	$17^h\ 41^m\ 24^s1$	-29° 15′ 51″	Sgr C
MC G−0.32−0.19	−0.32	−0.19	$17^h\ 42^m\ 24^s7$	-29° 17′ 20″	Sgr C
MC G−0.11−0.08	−0.11	−0.08	$17^h\ 42^m\ 28^s0$	-29° 02′ 55″	Sgr A
MC G−0.08−0.06	−0.08	−0.06	$17^h\ 42^m\ 30^s0$	-29° 00′ 58″	Sgr A
MC G−0.02−0.07	−0.02	−0.07	$17^h\ 42^m\ 40^s0$	-28° 58′ 00″	Sgr A
MC G+0.04+0.03	+0.04	+0.03	$17^h\ 42^m\ 26^s2$	-28° 51′ 45″	TRA
MC G+0.07−0.07	+0.07	−0.07	$17^h\ 42^m\ 54^s2$	-28° 53′ 30″	TRA
MC G+0.13+0.02	+0.13	+0.02	$17^h\ 42^m\ 41^s4$	-28° 47′ 35″	TRA
MC G+0.17+0.01	+0.17	+0.01	$17^h\ 42^m\ 50^s0$	-28° 45′ 50″	TRA
MC G+0.18−0.04	+0.18	−0.04	$17^h\ 43^m\ 01^s0$	-28° 47′ 15″	Sickle
MC G+0.20−0.03	+0.20	−0.03	$17^h\ 43^m\ 03^s6$	-28° 45′ 42″	Sickle
MC G+0.24+0.01	+0.24	+0.01	$17^h\ 42^m\ 59^s6$	-28° 42′ 35″	Sickle
MC G+0.62−0.10	+0.62	−0.10	$17^h\ 44^m\ 18^s0$	-28° 26′ 30″	Sgr B2_a
MC G+0.64−0.08	+0.64	−0.08	$17^h\ 44^m\ 17^s5$	-28° 24′ 30″	Sgr B2_a
MC G+0.67−0.06	+0.67	−0.06	$17^h\ 44^m\ 18^s0$	-28° 22′ 30″	Sgr B2_a
MC G+0.68−0.10	+0.68	−0.10	$17^h\ 44^m\ 27^s2$	-28° 23′ 20″	Sgr B2_a
MC G+0.70−0.01	+0.70	−0.01	$17^h\ 44^m\ 10^s0$	-28° 19′ 30″	Sgr B2_a
MC G+0.70−0.09	+0.70	−0.09	$17^h\ 44^m\ 27^s2$	-28° 22′ 05″	Sgr B2_a
MC G+0.71−0.13	+0.71	−0.13	$17^h\ 44^m\ 38^s4$	-28° 22′ 25″	Sgr B2_a
MC G+0.76−0.05	+0.76	−0.05	$17^h\ 44^m\ 27^s2$	-28° 17′ 35″	Sgr B2_a
SGR B2N	+0.68	−0.03	$17^h\ 44^m\ 10^s6$	-28° 21′ 17″	Hot Core
SGR B2M	+0.66	−0.04	$17^h\ 44^m\ 10^s6$	-28° 22′ 05″	Hot Core
MC G+0.694−0.017	+0.694	−0.017	$17^h\ 44^m\ 10^s0$	-28° 20′ 05″	Sgr B2
MC G+0.693−0.027	+0.693	−0.027	$17^h\ 44^m\ 12^s1$	-28° 20′ 25″	Sgr B2
MC G+0.627−0.067	+0.627	−0.067	$17^h\ 44^m\ 12^s1$	-28° 25′ 05″	Sgr B2
MC G+0.630−0.072	+0.630	−0.072	$17^h\ 44^m\ 13^s6$	-28° 25′ 05″	Sgr B2
MC G+0.672−0.014	+0.672	−0.014	$17^h\ 44^m\ 06^s1$	-28° 21′ 05″	Sgr B2
MC G+0.640−0.046	+0.640	−0.046	$17^h\ 44^m\ 09^s1$	-28° 23′ 45″	Sgr B2
MC G+0.635−0.069	+0.635	−0.069	$17^h\ 44^m\ 13^s6$	-28° 24′ 45″	Sgr B2
MC G+0.659−0.035	+0.659	−0.035	$17^h\ 44^m\ 09^s1$	-28° 22′ 25″	Sgr B2
MC G+0.681−0.028	+0.681	−0.028	$17^h\ 44^m\ 10^s6$	-28° 21′ 05″	Sgr B2
MC G+0.673−0.025	+0.673	−0.025	$17^h\ 44^m\ 09^s1$	-28° 21′ 25″	Sgr B2

Note. Galactic and equatorial coordinates of the selected sources. Nomenclature, as recommended by the IAU: MC followed by a G and the galactic coordinates, where MC stands for Galactic center molecular cloud. We have grouped the sources by regions: sources around Sgr C, Sgr A, the TRA, the Sickle, Sgr B2 (_a is to difference two observation sessions), and the hot cores. Not all sources in the TRA or in the Sickle are affected by the same physical conditions.

but different intensities due to the nuclear spin degeneracy. These substates are called AA, EE, EA, and AE. Since the four substates are blended, we measured the integrated intensity of the four substates and then summed all the spin weights of each substate to derive the $(CH_3)_2O$ column densities.

– To obtain the upper limits to the column densities of undetected transitions like those of CH_3COOH, we used the 3σ level for the integrated intensities.

Derived parameters from the Gaussian fits (peak intensity, integrated intensity, radial velocity and linewidth) for all transitions in each source are shown electronically in Table **??**, available at the CDS.

The linewidths of the complex organic molecules in our sources are ~15 km s^{-1}, typical in the GC region. Radial veloc-

ities of the different sources range from −93 km s^{-1} to 140 km s^{-1}.
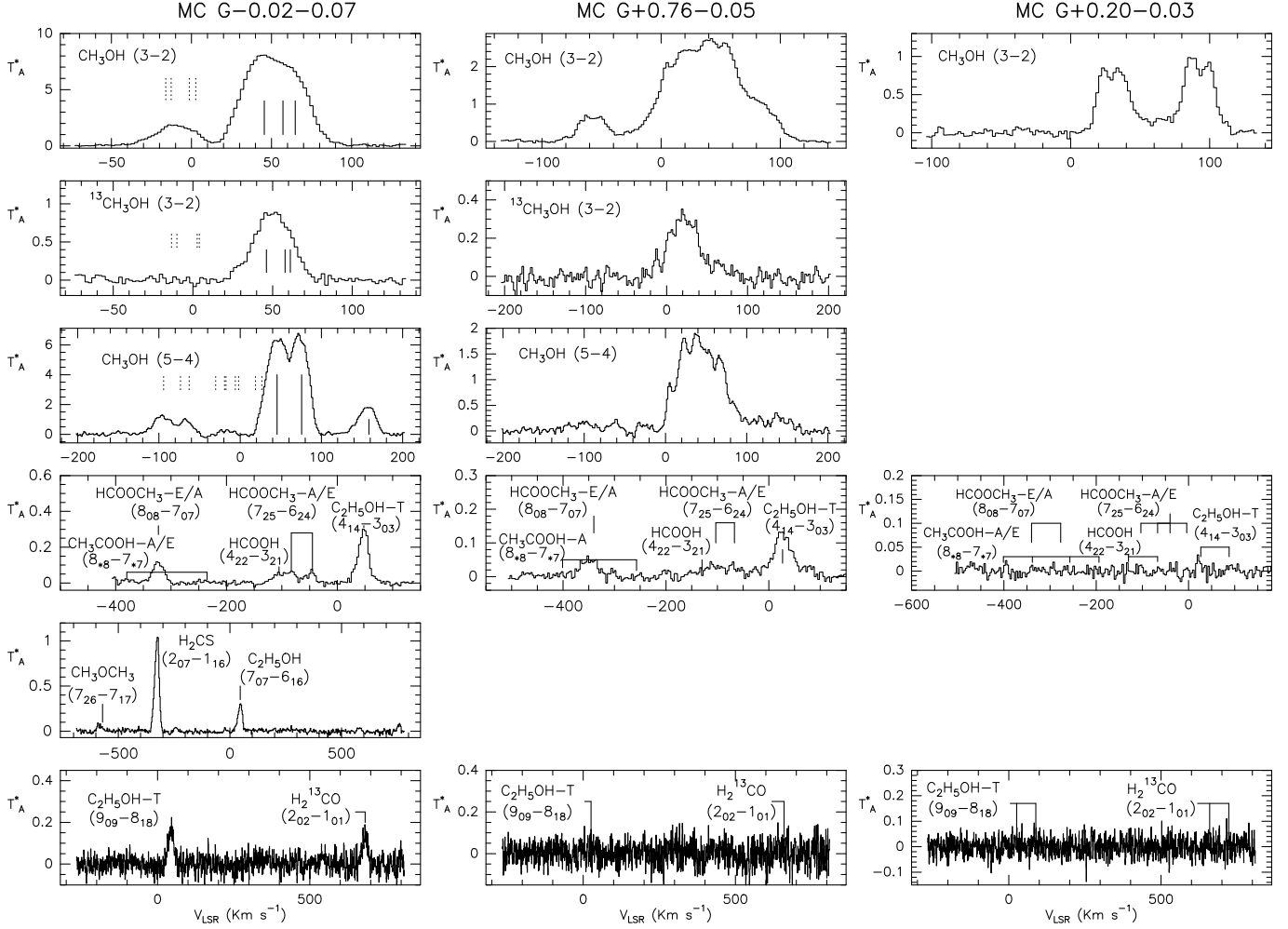
4. Derived parameters

4.1. Column densities, excitation temperatures, and densities

Molecular column densities were derived by assuming optically thin emission and the local thermodynamic equilibrium (LTE) approximation. In the case of optically thick lines like those of CH_3OH, the optically thin isotopic substitution was used. Under these conditions, the total column density, N, of a molecule is given by:

$$N = \frac{N_u}{g_u g_i} Q e^{(E_u/\kappa T_{rot})} \tag{1}$$

Table 3. Dipole moments and rotational constants of the observed molecules

| molecule	μ_a (Debye)	μ_b (Debye)	A (MHz)	B (MHz)	C (MHz)	Q	comments	references
CH_3OH	0.885	1.440	127484.00	24679.98	23769.70	$1.28\,T_{rot}^{1.5}$	Rotational levels split into E and A substates. Observed transitions with several blended lines.	Menten et al. (1986) Anderson et al. (1990a)
$^{13}CH_3OH$	0.899	1.440	127527.40	24083.50	23197.00	$1.28\,T_{rot}^{1.5}$	Rotational levels split into E and A substates. Observed transitions with several blended lines.	Anderson et al. (1990b) Xu & Lovas (1997)
C_2H_5OH	0.046	1.438	34891.77	9350.68	8135.34	$3.2\,T_{rot}^{1.5}$	Rotational levels split into Trans and Gauche substates. Only Trans Transitions are exited at $\sim 10\,K$.	Pearson et al. (1995, 1997)
$HCOOCH_3$	1.630	0.680	19985.71	6914.75	5304.48	$12.45\,T_{rot}^{1.5}$	Rotational levels split into E and A substates.	Plummer et al. (1984, 1986) Kuan & Snyder (1996)
$(CH_3)_2O$	0.000	1.302	38788.20	10056.50	8886.80	$91.6\,T_{rot}^{1.5}$	Rotational levels spilt into AA, EE, AE and EA substates. g_i: (K_aK_c: $ee \leftrightarrow oo$) AA:EE:AE:EA=6:16:2:4 g_i: (K_aK_c: $oe \leftrightarrow eo$) AA:EE:AE:EA=10:16:6:4	Groner et al. (1998)
$HCOOH$	1.396	0.260	77512.25	12055.11	10416.12	$1.68\,T_{rot}^{1.5}$		Willemot et al. (1980) Liu et al. (2002)
CH_3COOH	0.860	1.470	11335.58	9478.73	5324.99	$14.1\,T_{rot}^{1.5}$	Rotational levels split into E and A substates.	Wlodarczad & Demaison (1988) Mehringer et al. (1997)
$H_2^{13}CO$	2.332		281993.04	37809.11	33215.94	$0.57\,T_{rot}^{1.5}$	Para (K_a=e) and Orto (K_a=o) split, $g_i \rightarrow$ 1(p)-3(o).	Johnson et al. (1972)
CS	1.957			24495.56		$0.84\,T_{rot}$		JPL
$C^{18}O$	0.111			54891.42		$0.38\,T_{rot}$		JPL
^{13}CO	0.111			55101.01		$0.38\,T_{rot}$		JPL

Fig. 2. Observed line profiles toward the sources MC G−0.02−0.07, MC G+0.76−0.05, and MC G+0.20−0.03. Line intensities are expressed in antenna temperature (K), and velocities refer to LSR (km s^{-1}). The CH$_3$OH profiles are composed of several overlapped transitions arising from levels with different energies; in the MC G−0.02−0.07 source, we show the transitions with highest intensities as vertical solid lines and the transitions with lowest intensities as dotted lines. These transitions are: for CH$_3$OH J=3→2, from left to right, $3_2→2_2$A, $3_1→2_1$E, $3_{-2}→2_{-2}$E, $3_2→2_2$E, $3_2→2_2$A-, $3_0→2_0$A+, $3_{-1}→2_{-1}$E, and $3_0→2_0$E. For the ^{13}CH$_3$OH J=3→2, from left to right, $3_{21}→2_{20}$A+, $3_{12}→2_{11}$E, $3_{21}→2_{21}$E, $3_{-22}→2_{-21}$E, $3_{22}→2_{21}$A-, $3_{03}→2_{02}$A+, $3_{-13}→2_{-12}$E, and $3_{03}→2_{02}$E. For the CH$_3$OH J=5→4 from left to right; $5_2→4_2$E, $5_{-2}→4_{-2}$E, $5_2→4_2$A+, $5_1→4_1$E, $5_{-3}→4_{-3}$E, $5_3→4_3$E, $5_2→4_2$A-, $5_3→4_3$A-, $5_3→4_3$A+, $5_4→4_4$E, $5_{-4}→4_{-4}$E, $5_4→4_4$A-, $5_4→4_4$A, $5_0→4_0$E, $5_{-1}→4_{-1}$E, and $5_0→4_0$E. All these transitions have been used for the multi-Gaussian fit. The spectrum toward MC G+0.20−0.03 shows two velocity components.

$$N_{\rm u} = 1.67 \times 10^{14} \frac{g_{\rm u}}{\nu\mu^2 S} \int T_{\rm A}^* dv \,, \qquad (2)$$

where N$_u$ is the column density in the upper level of the observed transition in cm^{-2}, g_u the upper level degeneracy (2J$_u$+1), ν the line frequency in GHz, μ the dipole moment in Debye, S the line strength, $\int T_A^* dv$ the integrated intensity in K km s^{-1}, g_i the spin weight degeneracy, Q the partition function, E_u/κ the upper level energy in K, and $T_{\rm rot}$ the rotational temperature also in K. Table 3 summarizes the dipole moments, the rotational constants, the partition functions, and the statistical weights used to calculate the total column densities.

4.1.1. Rotational temperatures

To derive the total column densities one first needs to estimate $T_{\rm rot}$. For molecules with more than one observed transition, we calculated $T_{\rm rot}$ from population diagrams. Figure 4 shows, as an example, the population diagrams ($ln(N_{\rm u}/g_{\rm u})$ vs. $E_{\rm u}/\kappa$) of some of the organic complex molecules derived for the source MC G−0.02−0.07. In general, $T_{\rm rot}$ from different molecules (third column on Table 6) agree within a factor of 2. We find $T_{\rm rot}$ values between 6 K and 18 K, much lower than the typical kinetic temperatures of $\gtrsim$100 K derived from NH$_3$ by Hüttemeister et al. (1993a) and H$_2$ by Rodríguez-Fernández et al. (2000, 2001a), indicating subthermal excitation. We do not find any systematic trend in $T_{\rm rot}$ as a function of the molecule. For sources with only one observed transition, we assumed an average value of $T_{\rm rot}$ ~8 K.
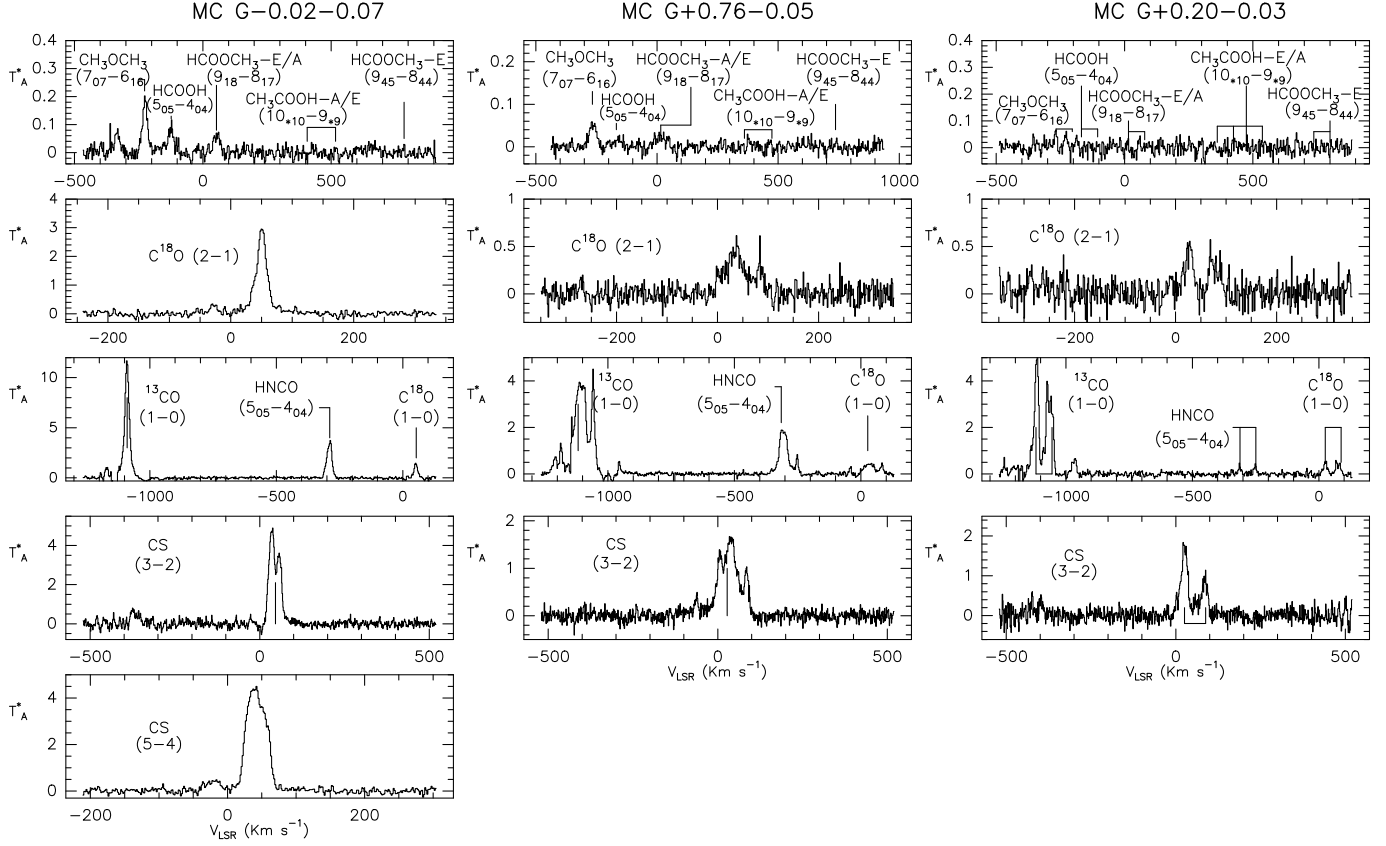
Fig. 3. Same as Fig. 2. The ^{13}CO, C^{18}O, and CS profiles show wider lines than those of the complex organic molecules in Fig. 2.

4.1.2. Densities

Once the T_{rot} is derived, we can make a rough estimate of the H$_2$ densities, providing that the kinetic temperatures and the collisional cross section are known. The H$_2$ densities can be estimated from

$$n = \frac{A_{ul}}{< v\sigma >_{ul}} \frac{1 + \left[1 - exp\left(\frac{h\nu}{\kappa T_{rot}}\right)\right] \frac{1}{exp\left(\frac{h\nu}{\kappa T_{bg}}\right) - 1}}{exp\left(\frac{h\nu}{\kappa T_{rot}}\right) exp\left(-\frac{h\nu}{\kappa T_k}\right) - 1} \qquad (3)$$

where A_{ul} is the Einstein coefficient between the upper and the lower levels, $<v\sigma>_{ul}$ the collisional rate coefficient between the same levels, ν the transition frequency, h the Plank constant, κ the Boltzmann constant, T_{rot} the rotational temperature, T_{bg} the background temperature, and T_k the kinetic temperature. Pottage et al. (2004) have calculated the collision rate coefficients ($<v\sigma>$) between E-CH$_3$OH and para-H$_2$ for kinetic temperatures between 5 K and 200 K. Assuming a kinetic temperature of 100 K (Hüttemeister et al. 1993a; Rodríguez-Fernández et al. 2001a), we obtain H$_2$ densities of $\sim 10^5$ cm^{-3} for the rotational temperature derived from CH$_3$OH of 6–18 K. Similar H$_2$ densities are also derived when the measured line intensities of E-CH$_3$OH are fitted using the large velocity gradient (LVG) approximation model, provided by J. Cernicharo, for the excitation of E-CH$_3$OH. We also estimated the H$_2$ densities from the excitation temperatures derived from C$_2$H$_5$OH. The collisional cross section in this case was estimated from those of CH$_3$OH but corrected for the difference in

mass and size. These roughly estimated H$_2$ densities are also $\sim 10^5$ cm^{-3}.

The derived H$_2$ densities are based on the collisional rates for a kinetic temperature of 100 K. However, the linewidths in the GC molecular clouds indicate the presence of supersonic turbulence and thus of non-equilibrium processes. In this case the collisional rates will not be described by the kinetic temperatures. However, for the observed transitions the rate coefficients do depend weakly on the increasing collisional velocities (Pottage et al. 2004), therefore our estimated densities will only be marginally affected by the effect of a larger velocity difference between the collisional partners than those represented by the kinetic temperature.

4.1.3. The H$_2$ column densities

To estimate the H$_2$ column density, we used the J=1→0 and J=2→1 C^{18}O and the J=1→0 ^{13}CO transitions using the LTE approximation. We used the isotopic ratios of ^{12}C/^{13}C= 20, ^{16}O/^{18}O= 250 (Wilson & Rood 1994), and a CO relative abundance of CO/H$_2$ = 10^{-4} (Frerking et al. 1982). The last column in Table 6 shows the derived H$_2$ column densities. Our H$_2$ column densities, derived from the LTE approximation, are within a factor of ≤2 of those derived by Rodríguez-Fernández et al. (2001a) using the LVG approximation.

Table 6 also shows the relative CS abundance estimated from the CS column densities derived using the T_{rot} obtained from CH$_3$OH. Since our data refer to the line emission of the
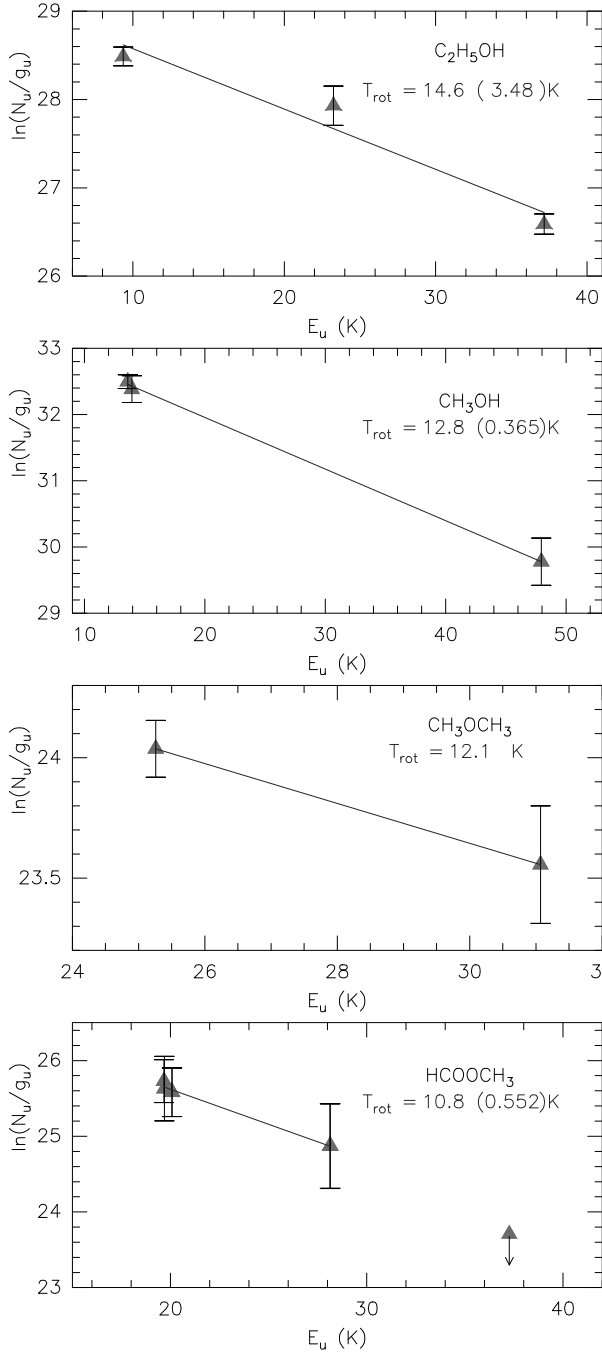
Fig. 4. Population diagrams for some complex molecules toward MC G−0.02−0.07. The error bars are derived by assuming a calibration uncertainty of 10% and the Gaussian fit error. Parentheses () indicate the calculated errors. Triangles with arrows represent upper limits to HCOOCH$_3$ column densities.

main CS isotopomer, optical depth effects might affect the derived CS column densities (Hüttemeister 1993b). We compared our results with those derived from ^{13}CS by Martín et al. (2006) in several common sources. The CS column densities derived from ^{13}CS are always higher than those of the CS by a factor of 1-5. When the ^{13}CS determinations are available, Table 6 shows the two values estimated for the relative abundance of CS.

4.1.4. Column densities of complex organic molecules

To derive the column densities of the complex organic molecules we used the parameters in Table 3 and Eqs. 1 and 2. The relative abundance of complex molecules derived from their column densities and the H$_2$ column densities are shown in Table 6.

4.2. Abundances and abundance ratios

Table 6 shows the derived rotation temperatures, fractional abundances, and the H$_2$ column densities for the different molecular clouds. Different sources in the same line of sight are identified by their radial velocities. The fractional abundances of the complex organic molecules are very high, even higher than in the hot cores. The abundances we find reach values up to 1.1×10^{-6} for CH$_3$OH, 6×10^{-8} for C$_2$H$_5$OH, 5.6×10^{-8} for (CH$_3$)$_2$O, 7.5×10^{-8} for HCOOCH$_3$, 4.1×10^{-9} for HCOOH, and 1.9×10^{-8} for H$_2$CO. We have only obtained upper limits to the abundance of CH$_3$COOH between $\leq 5 \times 10^{-10}$ and $\leq 5.5 \times 10^{-8}$.

There are some sources for which only upper limits to the abundances were measured for all the complex organic molecules except for CH$_3$OH. In some cases, like the sources with galactic longitude $\leq -0.30°$, the upper limits to the abundances of all complex molecules are not relevant because of the lack of sensitivity of our observations. In this case the upper limits have not been included in the discussion. Other cases, like the C$_2$H$_5$OH upper limits toward MC G+0.18−0.04, MC G+0.20−0.03 (Sickle), and MC G+0.13+0.02 (TRA) are relevant and therefore included in our discussion. The molecular emission toward the Sickle shows two velocity components at ∼25 km s^{-1} and ∼80 km s^{-1}, which are believed to be affected by the UV radiation produced by the Quintuplet cluster (Rodríguez-Fernández et al. 2001b). The molecular emission toward MC G+0.13+0.02, located in the TRA, also seems to be affected by the UV radiation from the Arches Cluster. In fact only the -30 km s^{-1} velocity component, which is clearly associated with the ionized gas (Serabyn & Güsten 1987), shows lower C$_2$H$_5$OH abundance than in other sources.

Because CH$_3$OH is the only molecule that has been detected in all sources and it is believed to play a central role in the formation of some of the observed complex organic molecules, we compared the abundances of the rest of the complex molecules with that of CH$_3$OH. Figure 5 summarizes the results illustrating the abundance of all the observed molecules relative to that of CH$_3$OH as a function of the CH$_3$OH abundance. As already mentioned, we have only included the significant upper limits in this figure. The main results are:

–In spite of the CH$_3$OH's abundance changing by a factor of ∼50, all the complex organic molecules, except that of the CH$_3$COOH with only upper limits to its abundance, show a surprisingly constant relative abundance with respect to CH$_3$OH.
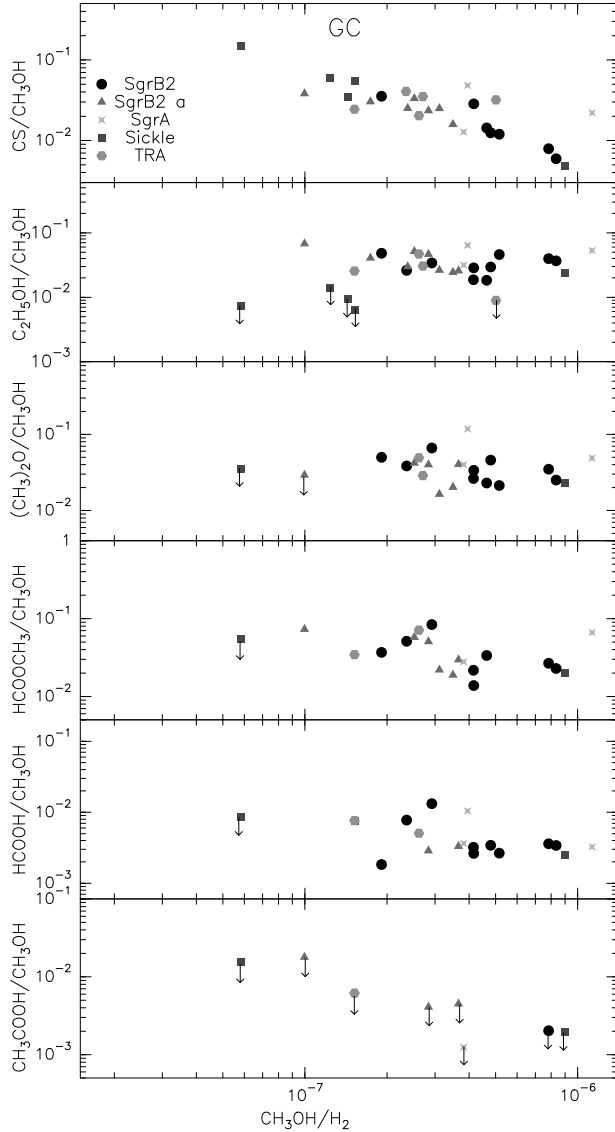
Fig. 5. Relative abundances of organic complex molecules with respect to CH_3OH as a function of the CH_3OH abundance for the selected GC clouds. Different regions are represented with different symbols (see Table 2). The arrows represent upper limits. Only the detections and significant upper limits are shown.
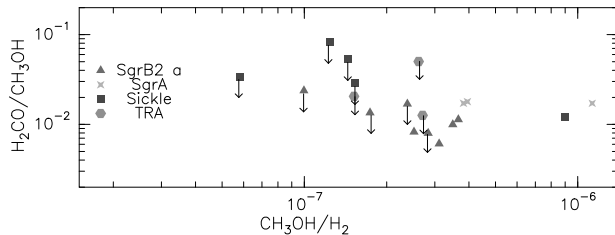
Fig. 6. Same as Fig. 5 but for H_2CO.

–The mean $[C_2H_5OH/CH_3OH]$ abundance ratio of $\sim 3.6 \times 10^{-2}$ is constant within a factor 3.7. The Sickle and the TRA clouds show upper limits to the $[C_2H_5OH/CH_3OH]$ ratios, which are a factor of $\gtrsim 6$ times lower than the mean ratio found in the typical GC clouds, a factor of $\gtrsim 1.6$ higher than

the scattering of the data.

–The abundance ratios $[(CH_3)_2O/CH_3OH]$ and $[HCOOCH_3/CH_3OH]$ present similar mean values of $\sim 3.9 \times 10^{-2}$. These ratios show a somewhat larger dispersion than that of C_2H_5OH but are constant within a factor of 7.

–For the $[HCOOH/CH_3OH]$ ratio, we obtained a mean value of $\sim 7.9 \times 10^{-3}$ and a dispersion of a factor of 5.3.

–CH_3COOH was not been detected in the GC clouds but its $[CH_3COOH/CH_3OH]$ ratio must be lower than 10^{-3}.

–We also show in Fig. 6 the $[H_2CO/CH_3OH]$ ratio as a function of the CH_3OH abundance. As for the more complex organic molecules, we find a constant ratio of $\sim 1.1 \times 10^{-2}$, within a factor 3.
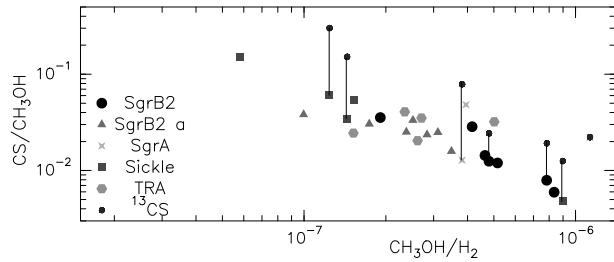
Fig. 7. Variation of $[CS/CH_3OH]$ as a function of CH_3OH abundances. The vertical bars show the changes due to the opacity.

The $[CS/CH_3OH]$ abundance ratio is shown in Fig. 7. This abundance ratio decreases by a factor 60 as the CH_3OH abundance increases. This is the only molecule for which we find a systematic trend, and the variation is clearly larger than those found for the complex organic molecules. As previously mentioned, our CS column densities could be affected by opacity effects. To show the effects of opacity, we have also included the abundance ratio obtained using the rarer CS isotopomer ^{13}CS in Fig. 7 as vertical bars. The $[CS/CH_3OH]$ abundance ratio derived from the optically thin isotopomer increases by a relatively constant value for all clouds independently of the CH_3OH abundance. The variation observed in the $[CS/CH_3OH]$ ratio as a function of the CH_3OH abundance, using the ^{13}CS data, is similar or even larger than that derived from the CS data. We therefore consider that the difference between the behavior of CS and the complex organic molecules is real and related to the different type of chemistry in the GC clouds.

5. Comparison with Galactic disk objects

In dark clouds, where the kinetic temperature is only 10 K, the abundance of complex organic molecules is very low. In the dark cloud TMC-1, the CH_3OH, H_2CO, and HCOOH abundances are as low as 2×10^{-9}, 2×10^{-8}, and 3×10^{-10}, respectively (see e.g. Turner 2000). For other dark clouds like L183,

one finds similar abundances of 8×10^{-9} for CH_3OH, of 2×10^{-8} for H_2CO, and of 3×10^{-10} for $HCOOH$ (Turner et al. 1999; Dickens et al. 2000). Other complex molecules, like C_2H_5OH, $(CH_3)_2O$, CH_3COOH, and $HCOOCH_3$, have not been detected so far, but model predictions suggest C_2H_5OH abundances of 10^{-12} (Hasegawa & Herbst 1993). High abundance of the complex organic molecules were first observed in the short-lived (10^{5-6} years) objects associated with massive star-forming regions known as hot cores. There, it is believed that grain mantle evaporation release complex molecules, like alcohols, into gas phase. Recently, Bottinelli et al. (2004a,b, 2006) and Kuan et al. (2004) detected relatively large abundances of complex organic molecules, like $HCOOCH_3$ and $(CH_3)_2O$, toward the so-called "hot corinos" associated with warm condensation surrounding low mass proto-stars.

In the following sections, we compare the abundances of complex organic molecules in the GC with those found in the hot cores and hot corinos associated with star formation.

5.1. Hot cores

For the comparison between the GC and hot cores associated to massive star formation, we selected the homogeneous data set by Ikeda et al. (2001) for several hot cores (W51, NGC6334f, G327.3−0.6, G31.41+0.31, G34.3+0.2, G10.47+0.03, and the Orion Hot Core). We also used data from Remijan et al. (2002, 2003) to obtain the CH_3COOH abundances derived from their $[HCOOCH_3/CH_3COOH]$ ratio. The hot cores abundances of complex molecules and the H_2 column densities are given in Table 4. Both the H_2 and molecular column densities were derived from observations with similar beam sizes. Then the derived fractional abundances are independent of beam dilution. Since our comparation is based on the relative abundance between complex molecules, our results are not affected by the size of the hot cores. We also used our data for the Sgr B2N and Sgr B2M hot cores in Table 6. Figure 8 illustrates the comparison between the abundance ratios observed for the GC and those measured in hot cores. As for the GC clouds, the abundance of CH_3OH in hot cores shows variations of more than one order of magnitude between different objects. Surprisingly, the abundance ratios relative to CH_3OH are also independent of the CH_3OH abundance and similar to those measured for the GC clouds. The C_2H_5OH and $HCOOH$ mean abundance ratios with respect to CH_3OH between hot cores and GC clouds are different by less than a factor of 2. The molecule that presents the largest difference in its abundance ratio with respect to that in the GC clouds is $(CH_3)_2O$ with a mean ratio of 2×10^{-1}, which is ∼6 times higher than those of the GC clouds. The $[CH_3COOH/CH_3OH]$ ratios in hot cores agree with the upper-limit ratios found in GC clouds. Our data for the Sgr B2N Hot Core shows slightly higher abundances of $HCOOCH_3$ and $HCOOH$ than the rest of the hot cores. The Sgr B2M Hot Core, with the lowest CH_3OH abundance, shows similar ratios to those in the GC sources.

It is remarkable that different objects like the hot cores and the GC clouds, with different properties in terms of densities,
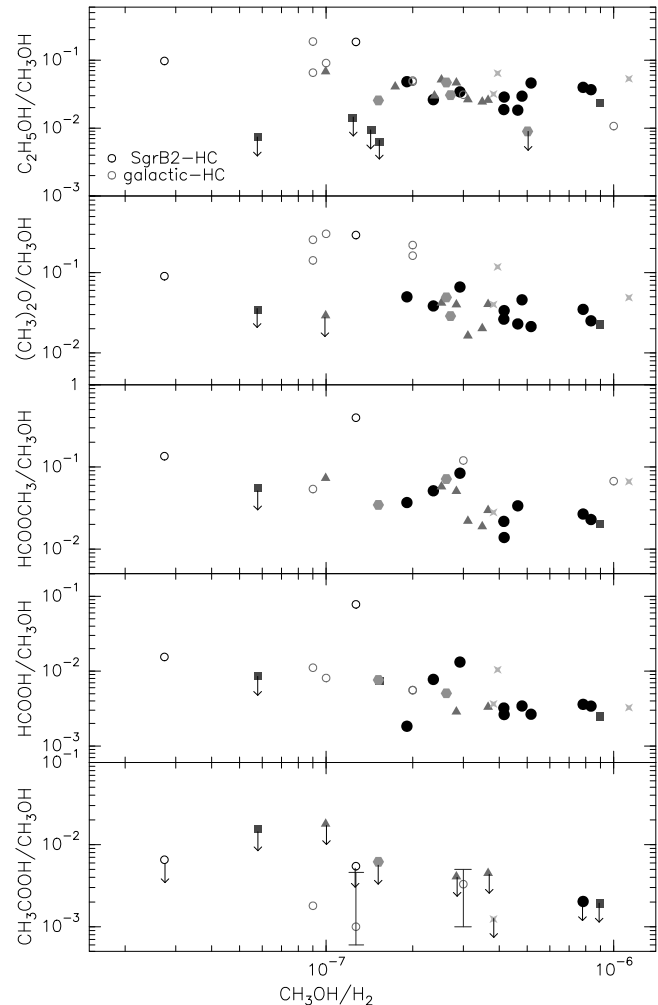
Fig. 8. Same as Fig. 5 but including the hot core abundances obtained from Ikeda et al. (2001), Remijan et al. (2002, 2003), and from our SGR B2 data as open symbols.

H_2 column densities, and spatial extension, show such uniform abundance ratios of very complex molecules. Hot cores are denser than the GC clouds by more than 2 orders of magnitude, and they typically have larger column densities than the GC clouds.

5.2. Hot corinos

Bottinelli et al. (2004a,b, 2006), Jørgensen et al. (2005) and Kuan et al. (2004) observed the hot corinos associated with the low mass proto-stars, NGC1333 IRAS 4A, NGC1333 IRAS 4B, NGC1333 IRAS 2A and IRAS 16293-2422 (A and B), which also show large abundances of $HCOOCH_3$, H_2CO, $(CH_3)_2O$ and $HCOOH$. Table 4 summarizes the recent compilation of the hot corino abundances of complex organic molecules by Bottinelli et al. (2006). In this case the molecular abundances were derived by assuming a source size of $0.5''$ for IRAS 4A (Bottinelli et al. 2004a), $0.25''$ for IRAS 4B, $0.43''$ for IRAS 2A (Maret et al. 2004), and $2''$ for IRAS 16293-2422 (Cazaux et al. 2003).

Table 4. Hot core abundances

source	X_{CH_3OH} $\times 10^{-7}$	$X_{C_2H_5OH}$ $\times 10^{-8}$	$X_{(CH_3)_2O}$ $\times 10^{-8}$	X_{HCOOCH_3} $\times 10^{-8}$	X_{HCOOH} $\times 10^{-9}$	X_{CH_3COOH} $\times 10^{-9}$	X_{H_2CO} $\times 10^{-8}$	$N(H_2)$ $\times 10^{22} cm^{-2}$
High mass[a]								
W51 e1/e2	3.0	0.9		3.0		0.3–1.8		36
NGC6334f	2.0	0.9	4.0		1.0			20
G327.3−0.6	1.0	1.0	3.0		0.9			20
G31.41+0.31	0.9	2.0	2.0		1.0			16
G34.3+0.2	0.9	0.6	1.0	0.5		0.2		30
G10.47+0.03	2.0	1.0	3.0		1.0			13
Omc HC	10.0	2.0		9.0				10
Low mass[b]								
IRAS 4A	≲0.1		≲2.8	6.8	4.6		2.0	160
IRAS 4B	7.0		≲120.0	220.0	≲1000		300.0	8.1
IRAS 2A	3.0		3.0	≲134.0	≲120		20.0	21
IRAS 16293	1.0		24.0	34.0	~62		10.0	7.5

[a] Ikeda et al. (2001) and Remijan et al. (2002, 2003).

[b] Bottinelli et al. (2006).

Except for IRAS 4A, which shows lower abundances, $HCOOCH_3$, $(CH_3)_2O$, $HCOOH$, and H_2CO show higher abundances in hot corinos than in the GC molecular clouds and hot cores. The data show that the abundance of CH_3OH varies between sources by nearly two orders of magnitude, similar to the variation observed in the GC clouds. As in the GC molecular clouds and in the hot cores, the abundance of the complex organic molecules relative to that of CH_3OH is independent of the CH_3OH abundance for different hot corinos (Bottinelli et al. 2006).

Although the number of observations of hot corinos is still limited, it seems that the abundance ratios, including species believed to be formed by different chemistries, show a similar behavior to the GC sources. However, the abundance of the molecules is very different, as expected if the grain mantle composition in dark clouds were different than in the GC clouds and hot cores.

6. Discussion

With the exception of the clouds associated with the Sickle and the TRA, large abundances of organic complex molecules like CH_3OH, C_2H_5OH, $(CH_3)_2O$, $HCOOCH_3$, $HCOOH$, and H_2CO seems to be a general characteristic of molecular clouds in the GC at scales of a few hundred parsecs. The main characteristic of the GC molecular gas is that the complex organic molecules show a constant relative abundance with respect to CH_3OH, within a factor 4–8 over the whole range of the CH_3OH abundances in the observed GC clouds. This contrasts with the [CS/CH_3OH] abundance ratio that increases by a factor of 60 when the CH_3OH abundance decreases.

We now discuss the origin of the chemistry of the complex molecules found in the GC sources, including the low [C_2H_5OH/CH_3OH] abundance ratio measured in the Sickle and the TRA clouds.

6.1. Models for gas-phase formations of organic molecules

Table 5 shows a compilation of the models proposed to explain the formation of complex organic molecules. Since gas-phase chemistry cannot account for the large abundance of alcohols, such as CH_3OH and C_2H_5OH, or for other organic molecules like the H_2CO measured in hot cores, evaporation from grain mantles has been proposed as the main formation mechanism. Most of these models assume that $(CH_3)_2O$ and $HCOOCH_3$ were produced in gas phase after the ejection of CH_3OH. However, it has been recently claimed that $HCOOCH_3$ cannot be produced efficiently in gas phase from CH_3OH (Horn et al. 2004). The large abundances of this molecule found in the GC clouds clearly indicate that $HCOOCH_3$ is hardly likely to be produced in gas phase. However, the most recent model from Peeters et al. (2006) studied the possibilities for the formation of $(CH_3)_2O$ on grain mantles and concluded that the gas-phase reactions are the dominant way to form $(CH_3)_2O$, while grain mantle reactions are the minor source.

From the theoretical point of view, so far, only $(CH_3)_2O$ seems to be produced in gas phase from reactions involving CH_3OH on relatively short time scales. Assuming that the gas phase models for the $(CH_3)_2O$ formation are correct (see references in Table 5), one would expect large changes in the relative abundances between the daughter ($(CH_3)_2O$) and parent (CH_3OH) molecules as a function of time after ejection/evaporation. One expects low [$(CH_3)_2O/CH_3OH$] abundance ratio in early times just when large abundances of CH_3OH are ejected into the gas phase and the gas phase processing starts. Low [$(CH_3)_2O/CH_3OH$] ratios are also expected in late times in the low CH_3OH abundance regime when an important fraction of CH_3OH has been converted into daughter molecules and both molecules have been destroyed by gas-phase reactions. Between these two regimes, one would expect the [$(CH_3)_2O/CH_3OH$] ratio to reach its maximum values, because the daughter molecules reach their maximum abundance.

Table 5. Summary of chemical models and observations of complex organic molecules

source	T (K)	n(H$_2$) (cm^{-3})	$\frac{C_2H_5OH}{CH_3OH}$[a] ×10^{-2}	$\frac{(CH_3)_2O}{CH_3OH}$[a] ×10^{-2}	$\frac{HCOOCH_3}{CH_3OH}$[a] ×10^{-2}	$\frac{H_2CO}{CH_3OH}$[a]	age ×10^{5}y
Galactic center clouds	~100[b]	~10^4-10^5	~3.66	~3.87	~3.96	~1.10×10^{-2}	
hot cores[c]	~100	~10^6	~6.90	~21.80	~8.03		
Leung et al. (1984)[d]	10	10^4	0.14	6.00		43.6	3.16
Herbst & Leung (1986)[e]	10	10^4	2.18	5.25		9.75	3.20
Herbst & Leung (1989)[e]	10	10^4	0.99	0.12		65.5	1.00
Millar et al. (1991)[d]	70	2×10^5	0.19	6.32×10^{-2}	1.26	1.18×10^3	1.60
Hasegawa & Herbst (1993)[f]	10	10^4	0.77	1.56×10^{-2}		4.06×10^2	3.20
Caselli et al. (1993)-CR[g]	100	10^6	1.5×10^{-4}	0.21	4.67×10^{-3}	1.05	1.00
Charnley et al. (1995)	100	2×10^6		~2	~1.5	4×10^{-2}	~0.30
Rodgers & Charnley (2001)[h]	100	10^7	3.75	30.00	10.00		0.12
Rodgers & Charnley (2001)[i]	100	10^7	20.00	12.50	0.50		0.60
Horn et al. (2004)[j]	100	10^6		0.75	3.33×10^{-2}	1.56	0.80
Peeters et al. (2006)[k]	100	10^7		50.00			0.20

[a] The relative abundances of C$_2$H$_5$OH, (CH$_3$)$_2$O, HCOOCH$_3$, and H$_2$CO with respect to CH$_3$OH predicted by time-dependent chemical models, refer to the age of maximum abundance of the CH$_3$OH's daughters.

[b] From Hüttemeister et al. (1993a) and Rodríguez-Fernández et al. (2001a).

[c] Mean abundance ratios for the hot core sources used in this work.

[d] Model 1 of the referred paper.

[e] Low-metal model in the referred paper.

[f] Model starting with all the H in H$_2$.

[g] Model fixed with the Orion Compact ridge observations.

[h] Model without NH$_3$.

[i] Model with NH$_3$.

[j] Model 3 of the referred paper.

[k] Model with (CH$_3$)$_2$O created only in gas phase.

From the hot core models, one expects variations in [(CH$_3$)$_2$O/CH$_3$OH] abundance ratio up to three orders of magnitude as a function of time. This contrasts with our data for the GC clouds and the hot cores, which show variations of less than one order of magnitude. Assuming that the chemical models for hot cores are applicable in the GC, the only possibility of explaining the high abundances of complex molecules and the rather constant [(CH$_3$)$_2$O/CH$_3$OH] abundance ratios is to consider that all GC clouds in our study, distributed over 200 pc, have undergone the ejection of CH$_3$OH from grain mantles nearly simultaneously, ~10^5 years ago. This possibility seems very unlikely, suggesting that (CH$_3$)$_2$O is also ejected from grain mantles. Since (CH$_3$)$_2$O shows similar abundances with respect to CH$_3$OH than the other molecules that can only be formed on grain mantles like C$_2$H$_5$OH and HCOOCH$_3$, our data support the scenario in which all complex organic molecules in the GC clouds, the hot cores, and also in hot corinos have been ejected/evaporated from grains.

Previously we also found differences in the behavior of the relative abundances of CS and the complex organic molecules. This behavior is supported by the data in shock regions associated with outflows, as in L1448 (Jiménez-Serra et al. 2005) and L1157 (Bachiller & Pérez Gutiérrez 1997). The CS abundance is enhanced by the shock, but the enhancement of CH$_3$OH is ~1 order of magnitude larger than that of CS. This effect of differential ejection of the molecules can explain the variation in the complex organic molecules abundances in gas phase, while the CS abundance remains marginally affected.

6.2. Grain mantle erosion by shocks and time scales for depletion

In the GC clouds, the typical dust-grain temperatures are low (T~10–30 K, Rodríguez-Fernández et al. 2004) and the ejection of molecules to gas phase cannot be produced by evaporation like in hot cores, but by shocks with moderate velocities. The shock heats the gas and produces the sputtering of molecules on the grain mantles. For shock velocities of ~20 km s^{-1}, the gas temperature can reach ~1000 K (Kaufman & Neufeld 1996). After the shock passage, the gas rapidly cools on time scales of ~10^4 years for densities of 10^5 cm^{-3}. The complex molecules ejected from the grains will again stick to the grains or grain mantles. The time scales will depend on the sticking coefficient. A sticking coefficient of ~1 is expected for mean velocities corresponding to the thermal velocity at temperatures of ≲200 K because the complex molecules will be absorbed after every collision with a grain (Tielens & Hagen 1982). However, the sticking coefficient decreases when increasing the relative velocity between the grains and the molecules (Leitch-Devlin & Williams 1985). Buch & Zhang (1991) and Masuda et al. (1998) estimated that the sticking coefficient of H is a function of the mean velocity.

The key parameter is the adsorption energy of the complex molecules, which will depend on the surface of the dust

grains. Since the CH_3OH abundance in gas phase is relatively large, grain mantles are completely eroded and the most likely grain surfaces in the GC clouds would be graphite and silicates. The absorption energy of CH_3OH on carbon basal planes is 1600 K (Aikawa et al. 1996) and on silicates is 2065 K (Allen & Robinson 1977). For the typical mean velocities in the GC of 2–4 km s^{-1} (see next section) the sticking coefficient will decrease and the time scale for sticking would be ~10^5 years on silicates and graphites. Similar time scales are found for the depletion of C_2H_5OH, $HCOOCH_3$, and $(CH_3)_2O$ molecules with absorption energies ~3000 K on silicates (Allen & Robinson 1977). Short time scales for depletion, like those expected in the GC, would require a mechanism that continuously ejects molecules from the grain mantles.

6.3. Origin of the shocks in the GC

Rodríguez-Fernández et al. (2001a, 2004) have summarized the possible mechanisms for the heating and the chemistry of the molecular gas in the GC. Turbulence and low-velocity shocks are proposed as the most likely mechanism for driving the chemistry. One of the key parameters for constraining the origin of the shocks is the velocity dispersion in the GC molecular clouds. High angular-resolution observation of the envelope of Sgr B2 indicates that the warm molecular gas is highly turbulent with linewidths of ~4 km s^{-1} (Martín-Pintado et al. 1999). Smith et al. (2000) show that MHD turbulence creates a wide range of shock velocities, but the larger amount of them should be produced with Mach numbers between 2–4. In the GC regions the sound speed is ~1 km s^{-1} (at 100 K), and then the more abundant shocks associated with turbulence should have velocities between 2 and 4 km s^{-1}, in agreement with the linewidth measured from high angular-resolution observations. As discussed in the previous section, for a mean velocity of ~3 km s^{-1}, the depletion will be ~10^5 years.

The energy of any kind of turbulence will decay if there is not any source injecting new energy. It is interesting to compare the depletion time scales with the turbulence decay time scales to establish if the turbulence can maintain mean velocities that are high enough to match the depletion time scales. The turbulence decays as $t^{-\alpha}$, where α~0.8–1.0 (Mac Low et al. 1998; Stone et al. 1998). The decay time scale of these turbulences is similar to one dynamical time ($t_{dyn}=L/\sigma_v$, where L is the turbulent length and σ_v the turbulent velocity, Avila-Reese & Vázquez-Semadeni 2001; Elmegreen & Scalo 2004), for both HD and MHD turbulence. The dynamical time for turbulence in the GC, assuming a turbulent length of 5 pc and a turbulent velocity dispersion of 15 km s^{-1} (observed GC linewidths), is ~3×10^5 years, close to the depletion time scale. Since we do not observe large depletions in our data, the existence of faster shocks with velocities high enough to produce the sputtering of the grain mantles and with the time scales between shocks similar to the time scales for depletion, ~10^5 years is required. Shocks with velocities of ≳6 km s^{-1} are required in order to sputter molecules from the icy mantles on graphite and silicate grains by heavy atoms (Draine & Salpeter 1979). Then, if due to a sudden event, the turbulence generated

by this event could explain the presence of complex organic molecules in the GC clouds for ~10^5 years.

It is so far unclear what produces the supersonic turbulence and/or frequent shocks in the GC. The high-velocity shocks and the presence of a highly turbulent medium in the GC could be due to: a) the kinematics of the gas subjected to the barred potential of our Galaxy, b) the wind-blown bubbles produced in evolved massive stars like supernovas, or c) cloud-cloud collisions. The time scales needed in the GC to maintain the large abundances are much smaller than those associated to the quasi-circular orbits (~1×10^7 years), and a large number of large scale shocks would be required to explain the observed properties of the complex molecules. The other possible mechanisms could explain the observations if cloud-cloud collision and energetic events driven by massive stars occur on time scales of 10^5 years. In the scenario of a recent star burst in the GC as proposed to explain the fine structure lines of ionized gas (Rodríguez-Fernández & Martín-Pintado 2005), frequent energetic events associated to massive stars are expected to produce shocks with moderate velocities of ~10 km s^{-1} (Martín-Pintado et al. 1999) ejecting complex molecules to gas phase and a large amount of energy into the ISM.

6.4. The chemistry of complex molecules in the Galaxy

The proposed gas-phase chemistry for some complex molecules does not seem to explain the similar abundances ratios observed in the GC clouds, in hot cores, and in hot corinos. From the empirical data gathered there, we can conclude that the most likely explanation for the large abundance of CH_3OH, $HCOOH$, $HCOOCH_3$, $(CH_3)_2O$ and C_2H_5OH is that all these molecules are ejected from grains. It is interesting to note that in this scenario, the ice-mantle composition in complex organic molecules in the GC and in hot cores must be very similar. This is surprising in view of the changes of the complex organic molecules abundances observed in the hot corinos. The presence of complex molecules on grains can be due to grain chemistry or to the depletion after formation in gas phase.

Further investigations of the abundance of organic molecules in dark clouds are needed to constrain the molecules formed on ice mantles by grain chemistry in different types of molecular clouds.

6.5. Sources with low C_2H_5OH abundances

We also observed some clouds where the relative abundance of some organic complex molecules like C_2H_5OH seems to be significantly smaller than expected from these observed in other sources in the GC. These sources are the Sickle (MC G+0.18+0.04 and MC G+0.20+0.03) and the -30 km s^{-1} velocity component of the TRA (MC G+0.13+0.02). We detected high CH_3OH abundances of ~10^{-7}, but only significant upper limits, ≲0.4-5×10^{-9} to the C_2H_5OH abundance. The stars from the Quintuplet and the Arches Clusters are said to heat and ionize the Sickle and the TRA (Rodríguez-Fernández et al. 2001b) creating

photodissociation-regions (PDRs) around them. In particular, the -30 km s^{-1} component is clearly associated with the TRA (Serabyn & Güsten 1987).

The chemistry in these sources is then expected to be strongly affected by the presence of the UV radiation. It is very likely that the complex molecules in these sources are ejected to gas phase by shocks with the same abundances as observed in other GC molecular cloud. Additional evaporation from grain mantles can be ruled out since the heating will require UV photons that will also destroy the complex molecules. Due to a large UV radiation-field, the relative abundance of the complex molecules will be affected by dissociation. One can make a rough estimate of the effects of the UV radiation on the molecular abundances by comparing their photodissociation rates. Using the UMIST RATE99 (Le Teuff et al. 2000) and the Ohio State University databases[1], we found that the photodissociation rates of $(CH_3)_2O$ and C_2H_5OH are larger than those of CH_3OH, HCOOH and H_2CO.

In Fig. 9 we show the results of a simple model in which we represent how the ejected complex organic molecules are photodestroyed as a function of time and visual extinction. The model considers a far-ultraviolet incident field 10^3 times higher than in the local ISM ($G_0=10^3$), which is the typical radiation field observed in GC PDRs (Rodríguez-Fernández et al. 2004). For the regions with low A_v, all the abundances decrease, but the abundance of C_2H_5OH decreases faster than the other organic complex molecules. Obviously the time scale for photodissociation depends on the visual extinction. We estimate a visual extinction of $A_v \sim 4$–17 mag for the Sickle and the TRA using our H_2 column densities in Table 6 and the conversion factor given by Bohlin (1975), A_v(mag)=$10^{-21} \times N_{H_2}$ (cm^{-2}). The photodissociation times scales for CH_3OH will be comparable to depletion time scales for an averaged visual extinction of ~ 8 mag.

For this visual extinction the other complex organic molecules will photodissociate much faster than the depletion time scale. This suggests that in the presence of UV radiation, large abundances of molecules like C_2H_5OH would require more frequent shocks than in the shielded regions. This is illustrated in Fig. 10, where we present the results of a simple model to show the time evolution of complex organic molecules in a region of $A_v=8$ mag. In this model, we consider the effects of the UV radiation on the complex molecules that have been ejected by periodic shocks of 5×10^4 years. They are ejected with the abundances measured in the GC and are destroyed because of the photodissociation. This simple model reproduces the constant high abundances observed for CH_3OH, while the abundances of C_2H_5OH can vary by ~ 3 orders of magnitude. In agreement with the observations, the photodissociation can reproduce the low abundances of C_2H_5OH in specific regions in the GC clouds. Further observation of complex organic molecules toward PDRs in the Galactic disk and in the Galactic center are required to test the proposed scenario.
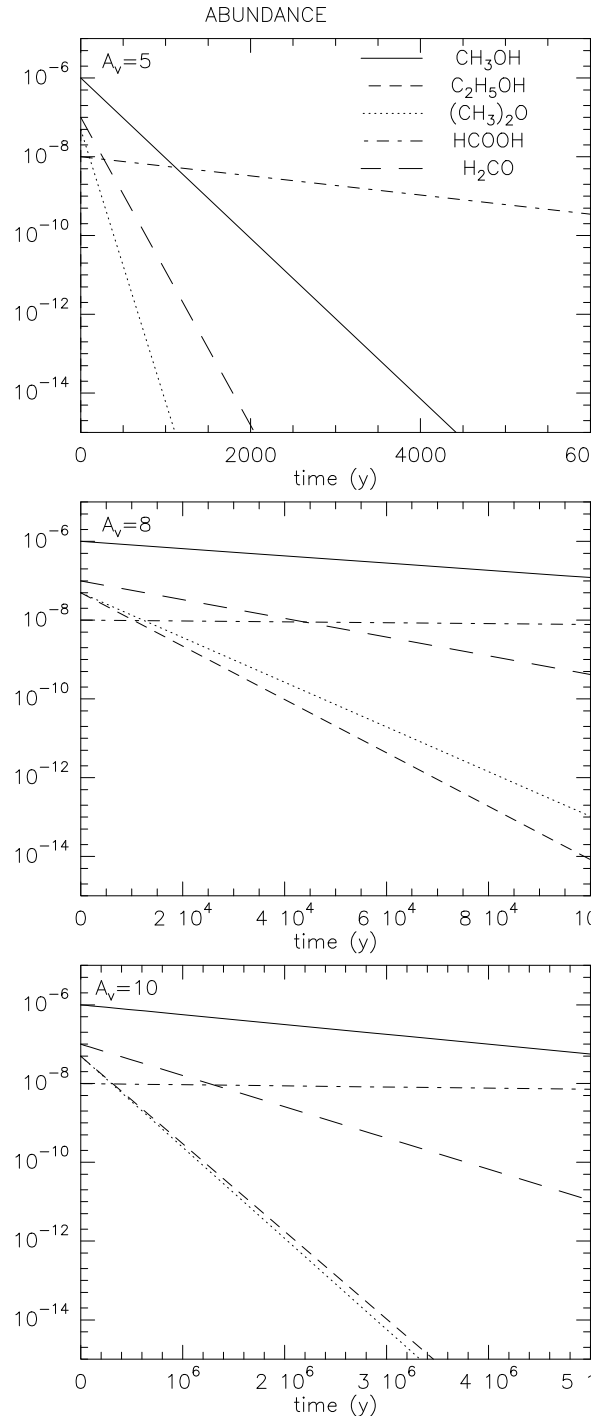
Fig. 9. Photodestruction of different complex molecules as a function of time for different visual extinctions (A_v). The initial molecular abundances for the molecules are considered to be those typically measured in the observed GC clouds. $G_0=10^3$, observed by Rodríguez-Fernández et al. (2004), is used for the UV radiation field.

7. Conclusion

We have found very high abundances for the complex organic molecules CH_3OH, C_2H_5OH, $HCOOCH_3$, $(CH_3)_2O$, and HCOOH in the GC regions, similar to or even higher than those measured in Galactic hot cores. The abundance ratios of these

---
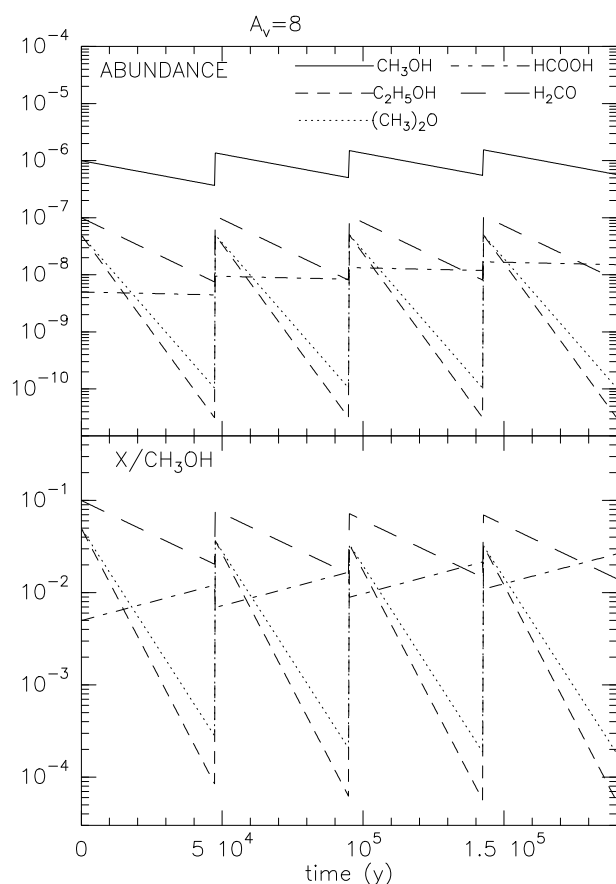
Fig. 10. Time evolution of the abundance (top) and relative abundance (bottom) of complex organic molecules with respect to that of CH_3OH in a PDR with $A_v=8$ mag where a periodic shock every 5×10^4 years enhances the abundances to their initial values. The radiation field is $G_0=10^3$.

molecules are fairly constant in all the GC clouds. The most likely explanation for these large abundances is that they have been ejected from grain mantles by shocks. The highly turbulent molecular clouds in the GC could help to maintain the large gas phase abundance of complex molecules for time scales of $\sim 10^5$ years after the ejection by shocks. The rather uniform abundance ratios in clouds distributed over 200 pc indicate that the average composition of grain mantles is similar for all the GC clouds and also for the hot cores in the Galactic disk. We found that, in the GC PDRs, UV photons can differentially photodissociate the complex molecules, changing their relative abundances dramatically.

References

Aikawa, Y., Miyama, S. M., Nakano, T., & Umebayashi, T. 1996, ApJ, 467, 684
Allen, M., & Robinson, G. W. 1977, ApJ, 212, 396
Anderson, T., de Lucia, F., & Herbst, E. 1990a, ApJ, 72, 797
Anderson, T., Herbst, E., & de Lucia, F. C. 1990b, ApJ, 74, 647
Avila-Reese, V., & Vázquez-Semadeni, E. 2001, ApJ, 553, 645
Bachiller, R., & Pérez Gutiérrez, M. 1997, ApJ, 487, L93
Bohlin, R. C. 1975, ApJ, 200, 402
Bottinelli, S., Ceccarelli, C., Lefloch, B. et al. 2004a, ApJ, 615, 354
Bottinelli, S., Ceccarelli, C., Neri, R. et al. 2004b, ApJ, 617, L69
Bottinelli, S., Ceccarelli, C., Williams, J. P., & Lefloch, B. 2006, A&A, submited
Buch, V., & Zhang, Q. 1991, ApJ, 379, 647
Caselli, P., Hasegawa, T. I., & Herbst, E. 1993, ApJ, 408, 548
Cazaux, S., Tielens, A. G. G. M., Ceccarelli, C., et al. 2003, ApJ, 593, L51
Charnley, S. B., Dress, M. E., Tielens, A. G. G. M., & Millar, T. J. 1995, ApJ, 448, 232
Draine, B. T., & Salpeter, E. E. 1979, ApJ, 231,438
Dickens, J. E., Irvine, W. M., Snell, R. L., et al. 2000, ApJ, 54, 870
Elmegreen, B. G., & Scalo, J. 2004, ARA&A, 42, 211
Frerking, M. A., Langer, W. D., & Wilson, R. W., 1982, ApJ, 262, 590
Gottlieb, C. A., Ball, J. A., Gottlieb, E. W., & Dickinson, D. F. 1979, ApJ, 227, 422
Groner, P., Albert, S., Herbst, E., & de Lucia, F. C. 1998, ApJ, 500, 1059
Güsten, R. & Philipp, S. 2004, astro-ph/0402019
Hasegawa, T. I., & Herbst, E. 1993, MNRAS, 261, 83
Hasegawa, T., Sato, F., Whiteoak, J. B., & Miyawaki, R. 1994, ApJ, 429, L77
Herbst, E., & Leung, C. M. 1986, MNRAS, 222, 689
Herbst, E., & Leung, C. M. 1989, ApJ, 69, 271
Horn, A., Møllendal, H., Sekiguchi, O. et al. 2004, ApJ, 611, 605
Hüttemeister, S., Wilson, T. L., Bania, T. M., & Martín-Pintado, J. 1993a, A&A, 280, 255
Hüttemeister 1993b, PhD dissertation, Bonn University
Hüttemeister, S., Dahmen, G., Mauesberer, R., Henkel, C., Wilson, T. L., & Martín-Pintado, J. 1998, A&A, 334, 646
Ikeda, M., Ohishi, M., Nummelin, A., Dickens, J. E. et al. 2001, ApJ, 560, 792
Jiménez-Serra, I., Martín-Pintado, J., & Rodríguez-Franco, A. 2005, ApJ, 627, L121
Johnson, D. R., Lovas, F., & Kirchhoff, W. H. 1972, J. Phys. Chem. Ref. Data, 1, 1972
Jørgensen, J. K., Schöier, F. L., & van Dishoeck, E. F. 2005, A&A, 437, 501
Kaufman, M. J., & Neufeld, D. A. 1996, ApJ, 456, 611
Kuan, Y.-J., & Snyder, L. E. 1996, ApJ, 470, 981
Kuan, Y.-J., Huang, H.-C., Charnley, S. B. et al. 2004, ApJ, 616, L27
Le Teuff, Y. H., Millar, T. J., & Markwick, A. J. 2000, A&AS, 146, 157
Leitch-Devlin, M. A., & Williams, D. A. 1985, MNRAS, 213, 295
Leung, C. M., Herbst, E., & Huebner, W. F. 1984, ApJS, 56, 231

Liu, S.-Y., Girart, J. M., Remijan, A. J., & Snyder, L. E. 2002, ApJ, 576, 255

Mac Low, M.-M., Dlessen, R. S., Burkert, A., & Smith, M. D. 1998, Phys. Rev. Lett., 80, 2754

Maret, S., Ceccarelli, C., Caux, E., et al. 2004, A&A, 416, 577

Martín et al. (2006) in preparation

Martín-Pintado, J., de Vicente, P., Fuente, A., & Planesas, P. 1997, ApJ, 482, L45

Martín-Pintado, J.,Gaume, R. A., Rodríguez-Fernández, N. J., de Vicente, P., & Wilson, T. L. 1999, ApJ, 519, 667

Martín-Pintado, J., Rizzo, J. R., de Vicente, P., Rodríguez-Fernández, N. J., & Fuente, A. 2001, ApJ, 548, L65

Masuda, K., Tkahashi, J., & Mukai, T. 1998, A&A, 330, 773

Mehringer, D. M., Snyder, L. E., & Miao, Y. 1997, ApJ, 480, L71

Menten, K. M., Walmsley, C. M., Henkel, C., & Wilson, T. L. 1986, A&A, 157, 318

Millar, T. J., Herbst, E., & Charnley, S. B. 1991, ApJ, 369, 147

Minh, Y. C., Irvine, W. M., & Friberg, P. 1992, A&A, 258, 489

Morris, M., & Serabyn, E. 1996, ARA&A, 34, 645

Pearson, J. C., Sastry, K. V. L. N., Winnewisser, M., Herbst, E., & de Lucia, F. C. 1995, J. Phys. Chem. Ref. Data, 24, 1

Pearson, J. C., Sastry, K. V. L. N., Herbst, E., & de Lucia, F. C. 1997, ApJ, 480, 420

Peeters, Z., Rodgers, S. D., Charnley, S. et al. 2006, A&A, 445, 197

Plummer, G. M., Herbst, E., de Lucia, F. C., & Blake, G. A. 1984, ApJ, 55, 633

Plummer, G. M., Herbst, E., de Lucia, F. C., & Blake, G. A. 1986, ApJ, 60, 949

Pottage, J. T., Flower, D. R., & Davis, S. L. 2004, MNRAS, 352, 39

Remijan, A., Snyder, L. E., Liu, S.-Y., Mehringer, D. M., & Kuan, Y.-J. 2002, ApJ, 576, 264

Remijan, A., Snyder, L. E., Friedel, D. N., Liu, S.-Y., & Shah, R.-Y. 2003, ApJ, 590, 314

Rodgers, S. D., & Charnley, S. B. 2001, ApJ, 546, 324

Rodríguez-Fernández, N. J., Martín-Pintado, J., de Vicente, P. et al. 2000, A&A, 356, 695

Rodríguez-Fernández, N. J., Martín-Pintado, J., Fuente, A., de Vicente, P., Wilson, T. L., & Hüttemeister, S. 2001a, A&A, 365, 174

Rodríguez-Fernández, N. J., Martín-Pintado, J., & de Vicente, P. 2001b, A&A, 377, 631

Rodríguez-Fernández, N. J., Martín-Pintado, J., Fuente, A., & Wilson, T. L. 2004, A&A, 427, 217

Rodríguez-Fernández, N. J., & Martín-Pintado, J. 2005, A&A, 429, 923

Rodríguez-Fernández, N. J., Combes, F., Martín-Pintado, J. Wilson, T. L., & Apponi, A. 2006, A&A, submited

Serabyn, E., & Güsten, R. 1987, A&A, 184, 133

Serabyn, E., & Güsten, R. 1991, A&A, 242, 376

Smith, M. D., Mac Low, M.-M., & Zuev, J. M. 2000 A&A, 356, 287

Stone, J. M., Ostriker, E. O., & Gammie, C. F. 1998, ApJ, 508, L99

Tielens, A. G. G. M., & Hagen, W. 1982, A&A, 114, 245

Turner, B. E., Terziava, R., & Herbst, E. 1999, ApJ, 518, 699

Turner, B. E. 2000, ApJ, 542, 837

Willemot, E., Dangoisse, D., Monnanteuil, N., & Bellet, J. 1980, JPCRD, 9, 59

Wilson, T. L., & Rood, R. T. 1994, ARAA, 32, 191

Wlodarczad, G., & Demaison, J. 1988, A&A, 192, 313

Xu, L.-H., & Lovas, F. L. 1997, JPCRD, 26, 17

Table 6. Relative abundances and H$_2$ column densities

source	V_{rad} (km s^{-1})	T_{rot} (K)	X_{CH_3OH} $\times10^{-7}$	$X_{C_2H_5OH}$ $\times10^{-8}$	$X_{(CH_3)_2O}$ $\times10^{-8}$	X_{HCOOCH_3} $\times10^{-8}$	X_{HCOOH} $\times10^{-9}$	X_{CH_3COOH} $\times10^{-9}$	X_{H_2CO} $\times10^{-9}$	X_{CS} $\times10^{-9}$	$N(H_2)$ $\times10^{22}$cm^{-2}
MC G−0.96+0.13	140	8.0[1]	10.6	≲ 1.4	≲ 8.3	≲10.7	≲12.2	≲30.0		16.6	0.2
MC G−0.55−0.05	−93	8.0[1]	1.6	≲ 1.8	≲ 0.6	≲ 2.7	≲ 1.0	≲ 8.5		3.6	1.5
MC G−0.50−0.03	−92	8.0[1]	0.4	≲ 1.0	≲ 0.3	≲ 1.1	≲ 0.4	≲ 3.6		1.6	2.5
MC G−0.42−0.01	−71	8.0[1]	0.6	≲ 1.9	≲ 0.6	≲ 2.9	≲ 1.1	≲ 9.5		3.5	0.6
MC G−0.32−0.19	−70.4	8.0[1]	0.9	≲ 0.8	≲18.1	≲ 6.2	≲23.4	≲17.5		10.0	0.2
MC G−0.32−0.19	−24	8.0[1]	0.2	≲ 0.6	≲ 6.3	≲ 4.5	≲17.0	≲12.7		7.3	0.2
MC G−0.32−0.19	26	8.0[1]	1.1	≲ 2.6	≲27.0	≲ 19.5	≲73.3	≲54.7		24.5	0.07
MC G−0.11−0.08	19.8	12.0[2]-10.0[1]	11.3	6.0	5.6	7.5	3.7	≲ 3.9	19.5	25.0/43.4 [3]	1.0
MC G−0.08−0.06	29.6	10.0[2]-12.0[1]	4.0	2.5	4.7	≲ 2.6	4.1	≲ 4.5	7.1	19.0	0.6
MC G−0.02−0.07	47	10.8[4]-14.0[2]	3.8	1.2	1.5	1.1	1.4	≲ 0.5	6.6	4.9/17.5 [3]	6.8
MC G+0.04+0.03	−26	10.0[1]	2.7	0.8	0.8	≲ 0.7	≲ 0.6	≲ 2.0	≲3.4	9.5	1.1
MC G+0.07−0.07	52	10.0[1]-12.8[2]	2.6	1.2	1.3	1.9	1.3	≲ 1.9	≲13.1	5.3	2.2
MC G+0.13+0.02	−30	8.0[5]	5.0	≲ 0.5	≲ 1.4	≲ 3.4	≲ 2.1	≲ 9.4		16.1	0.6
MC G+0.13+0.02	52	8.0[5]	2.4	≲ 0.5	≲ 1.6	≲ 3.7	≲ 2.4	≲10.5		9.6	0.4
MC G+0.17+0.01	59	10[1]-12.7[2]	1.5	0.4	≲ 0.3	0.5	1.2	≲ 0.9	≲3.1	3.7	1.3
MC G+0.18−0.04	27.1	8.0[5]	1.2	≲ 0.2	≲ 0.8	≲ 0.9	≲ 1.7	≲ 2.5	≲10.2	7.5/37.3 [3]	0.7
MC G+0.18−0.04	85.8	8.0[5]	1.4	≲ 0.1	≲ 0.6	≲ 0.7	≲ 1.3	≲ 1.9	≲7.8	5.0/22.0 [3]	0.8
MC G+0.20−0.03	24.9	8.0[5]	0.6	≲ 0.04	≲ 0.2	≲ 0.3	≲ 0.5	≲ 0.9	≲2.0	8.7	1.7
MC G+0.20−0.03	87.7	8.0[5]	1.5	≲ 0.09	≲ 0.4	≲ 0.7	≲ 1.1	≲ 2.0	≲4.4	8.3	0.9
MC G+0.24+0.01	36	12.6[2]-8.0[1]	9.0	2.1	2.1	1.8	2.3	≲ 1.7	10.9	4.3/11.3 [3]	3.0
MC G+0.62−0.10	56	11.0[2]-7.8[1]	3.5	0.8	0.7	0.7	≲ 0.3	≲ 1.1	3.5	5.5	2.6
MC G+0.64−0.08	63	10.0[21]	10.0	0.7	≲ 0.3	0.7	≲ 0.4	≲ 1.8	≲2.4	3.8	2.0
MC G+0.67−0.06	51	10.5[2]	3.1	0.8	0.5	0.7	≲ 0.4	≲ 1.3	1.9	7.8	3.1
MC G+0.68−0.10	21	9.0[2]-6.0[4]	2.5	1.3	1.1	1.5	≲ 0.4	≲ 1.3	2.1	8.4	3.2
MC G+0.70−0.01	62	11.0[2]-10.0[1]	3.7	0.9	1.5	1.1	1.2	≲ 1.6	4.2		2.8
MC G+0.70−0.09	43	10.0[1]	1.7	0.7	≲ 0.3	≲ 1.3	≲ 0.4	≲ 3.6	≲2.4	5.3	2.9
MC G+0.71−0.13	40	8.0[1]	2.4	≲ 0.8	≲ 0.6	≲ 2.8	≲ 0.9	≲ 7.9	≲0.6	6.0	2.8
MC G+0.76−0.05	27	10.0[14]	2.8	1.3	1.1	1.5	0.8	≲ 1.2	≲2.3	6.7	3.8
MC G+0.694−0.017	66	8.0[1]-11.0[4]	8.3	3.1	2.1	1.9	2.8	≲ 2.4		5.0	3.9
MC G+0.693−0.027	68	10.0[1]-11.5[4]	7.8	3.1	2.7	2.1	2.8	≲ 1.6		6.2/15.0 [3]	4.1
MC G+0.627−0.067	49	10.0[1]-6.0[4]	4.8	1.4	2.2	≲ 0.8	1.6	≲ 2.2		6.0/11.7 [3]	2.2
MC G+0.630−0.072	46	9.0[1]-12.0[6]	5.2	2.4	1.1	≲ 0.9	1.4	≲ 2.5		6.2	1.4

[1] Derived from CH$_3$OH.
[2] Derived from C$_2$H$_5$OH.
[3] From ^{13}CS (Martín et al. 2006).
[4] Derived from HCOOCH$_3$.
[5] Assumed 8 K.
[6] Derived from (CH$_3$)$_2$O.

Table 6. Relative abundances and H$_2$ column densities

source	V_{rad} (km s^{-1})	T_{rot} (K)	X_{CH_3OH} ×10^{-7}	$X_{C_2H_5OH}$ ×10^{-8}	$X_{(CH_3)_2O}$ ×10^{-8}	X_{HCOOCH_3} ×10^{-8}	X_{HCOOH} ×10^{-9}	X_{CH_3COOH} ×10^{-9}	X_{H_2CO} ×10^{-9}	X_{CS} ×10^{-9}	N(H$_2$) ×10^{22}cm^{-2}
MC G+0.672−0.014	54	10.0[14]	1.9	0.9	1.0	0.7	0.4	≲ 1.2		6.8	5.5
MC G+0.640−0.046	58	10.0[1]-7.0[6]	4.2	1.2	1.4	0.6	1.1	≲ 1.6		11.9	4.7
MC G+0.635−0.069	48	11.0[6]-8.0[4]	4.6	0.9	1.1	1.6	≲ 0.6	≲ 2.5		6.7	2.3
MC G+0.659−0.035	62	11.0[1]-16.0[4]	4.2	0.8	1.1	0.9	1.3	≲ 0.7			13.9
MC G+0.681−0.028	65	11.0[1]-12.0[4]	2.9	1.0	1.9	2.5	3.9	≲ 0.8			8.8
MC G+0.673−0.025	68	18.5[4]-13.9[1]	2.4	0.6	0.9	1.2	1.8	≲ 0.8			14.6
SGR B2N	65	72.6[2]	1.3	2.3	3.5	5.0	9.9	≲ 0.7			19.0
SGR B2M	63	55.4[2]	0.3	0.3	0.3	0.4	0.4	≲ 0.2			65.0